Research on Engineering Structures & Materials
www.jresm.org
Research Group

Research Article

Cracking behavior of partially prestressed concrete pier caps: Field evidence, nonlinear modeling, and implications for code-based crack control

Viet-Hung Cu [1,a], Phuc-Thanh Trinh [1,2,b], Thi-Nguyet-Hang Nguyen [1,c], Van-Tuan Hoang [1,d], Cong-Vinh Tran [1,e], Viet-Hung Tran[*,1,f]

[1]*Faculty of Bridge and Road Engineering, Hanoi University of Civil Engineering, Hanoi, Vietnam*
[2]*School of Civil Engineering, Beijing Jiaotong University, Beijing, China*

Article Info

Article History:

Received 03 Mar 2026

Accepted 09 June 2026

Keywords:

Partial prestressing;
Bridge pier caps;
Serviceability cracking;
Finite element method;
Fracture-based modeling

Abstract

Partially prestressed concrete (PPC) is widely used in bridge substructures because it combines the stiffness of prestressing with the ductility of reinforced concrete. However, current crack control provisions are largely derived from reinforced or fully prestressed concrete and have not been validated for PPC members under real service conditions. This study investigates the cracking behavior of 113 in-service PPC pier caps from the Ben Luc – Long Thanh Expressway in Vietnam through field measurements, nonlinear finite element analysis, and code-based evaluation. Field inspections revealed that cracking occurred in 87 pier caps, with maximum crack widths reaching 0.545 mm and crack depths exceeding the 50 mm concrete cover, indicating a potential durability concern despite full compliance with AASHTO LRFD and ACI 318 crack control requirements. A three-dimensional nonlinear finite element model incorporating concrete fracture mechanics and prestress–crack interaction predicted a maximum crack width of 0.448 mm and reproduced the observed crack localization at pier–cap junctions and bearing regions. Comparisons with ACI 224R and AASHTO LRFD formulations show that standard empirical models may underestimate crack widths, in some cases by more than 40%. This discrepancy is attributed to the distinctive cracking mechanism of PPC, in which prestressing tends to suppress distributed multiple cracking while promoting strain localization and wider individual cracks. The results suggest that current crack control provisions may be non-conservative for PPC pier caps and that nonlinear fracture-based analysis offers a more reliable basis for serviceability assessment.

1. Introduction

Partially prestressed concrete (PPC) was introduced as a hybrid structural system combining the crack tolerance and ductility of reinforced concrete (RC) with the stiffness and serviceability advantages of fully prestressed concrete (FPC) [1-5]. By allowing limited tensile cracking under service loads, PPC members can reduce excessive camber and creep typical of FPC while maintaining superior post-cracking stiffness compared with RC [2-4, 6, 7]. These advantages have led to the increasing use of PPC in bridge components such as beams, pier caps, and deep members.

Despite its practical importance, the serviceability design of PPC remains less well defined than that of RC or FPC. While RC design permits cracking and FPC design aims to avoid it, PPC occupies an intermediate regime in which cracking is allowed but must be strictly controlled to prevent

[*]Corresponding author: hungtv@huce.edu.vn
[a]orcid.org/ 0009-0003-7481-3821; [b]orcid.org/ 0009-0005-1654-9430; [c]orcid.org/ 0000-0002-6449-6055; [d]orcid.org/ 0000-0003-4161-2196; [e]orcid.org/ 0009-0007-3459-2656; [f]orcid.org/ 0000-0003-2690-1379
DOI: http://dx.doi.org/10.17515/resm2026-1542me0303rs

durability problems such as reinforcement corrosion and surface deterioration [8, 9]. However, current design standards, including ACI 318 and AASHTO LRFD, do not provide crack control provisions specifically developed for PPC members. Instead, they rely on crack width formulas and reinforcement spacing rules originally derived for RC or fully bonded prestressed concrete.

Experimental and analytical studies have demonstrated that PPC exhibits cracking behavior that is distinct from that of RC. Witchukreangkrai [8] showed that cracking in PPC beams is governed by the interaction between prestressing and conventional reinforcement. Harajli and Naaman [3] and Chern et al. [2] reported that progressive cracking and stress redistribution in PPC depend on the balance between prestress and applied loads. Furthermore, the partial prestressing ratio (PPR) has a distinct impact on cracking behavior: a decrease in PPR results in reduced crack spacing and narrower crack widths [10]. More recent studies have shown that standard crack width formulas and serviceability models fail to predict cracking and deflection once decompression is exceeded, particularly under repeated loading [10-12]. Advanced research has established a correlation between the flexural stiffness degradation of cracked sections and crack width. Newly proposed equations facilitate crack width prediction by integrating strain compatibility, the partial prestressing ratio (PPR), the location of the non-prestressed reinforcement centroid, and the concrete cracking stress, thereby demonstrating improved accuracy when validated against experimental data [10]. In addition, deep members have been shown to exhibit crack development governed by internal strain energy rather than simple stress limits [13], and higher-strength concrete may even lead to wider cracks due to increased brittleness [14].

Advances in numerical modeling further indicate that cracking in prestressed and partially prestressed members is governed by nonlinear fracture processes that cannot be captured by empirical equations. Parametric studies [15] and fracture-based simulations [16] have demonstrated large discrepancies between code predictions and actual crack widths, while Accornero et al. [17] highlighted the importance of modeling the transition from distributed cracking to localized fracture in prestressed concrete. In addition, Liu et al. [18] developed a machine learning model utilizing a boosting framework to predict the maximum crack width in partially prestressed concrete (PPC) beams. Building upon these predictive capabilities, the authors introduced a rapid design methodology governed directly by crack width limitations.

However, most of the available evidence is derived from laboratory tests on beams under controlled loading conditions [3, 10, 14, 18]. Field-scale data from in-service PPC bridge components remain extremely limited, particularly for members designed to be crack-controlled according to ACI and AASHTO provisions. As a result, the reliability of current design rules has not been verified under real service conditions. Consequently, it remains unclear whether the crack control provisions embedded in ACI 318, ACI 224, and AASHTO LRFD [19] are conservative, adequate, or unsafe when applied to real PPC bridge structures.

This study addresses this gap by investigating the cracking behavior of 113 partially prestressed concrete pier caps from the Ben Luc – Long Thanh Expressway in Vietnam. These pier caps were designed in accordance with AASHTO LRFD and ACI-based crack control provisions, providing a unique opportunity to evaluate the real-world performance of current design rules. A detailed field survey was conducted to measure crack locations, widths, and depths under service conditions. In addition, a three-dimensional nonlinear finite element model based on concrete fracture mechanics was developed to simulate crack initiation, propagation, and reopening under combined prestress and service loads.

The objectives of this study are to *(i)* establish a large-scale field dataset describing the actual cracking behavior of PPC pier caps, *(ii)* evaluate the ability of nonlinear fracture-based finite element modeling to reproduce observed cracking patterns and magnitudes, and *(iii)* assess the adequacy of current ACI and AASHTO crack control provisions for PPC bridge substructures. By linking field observations, numerical simulations, and code-based predictions within a unified framework, this study demonstrates that the cracking mechanism of PPC differs fundamentally from that assumed in current design standards, and that spacing-based crack control may be insufficient for PPC members. The findings provide new physical insight into PPC serviceability

behavior and support the need for fracture-based design approaches for durability-critical bridge components.

2. Description of the PPC Pier Caps and Field Survey

2.1. Structural Configuration of the PPC Pier Caps

The present study investigates 113 PPC pier caps forming part of the elevated viaduct of the Ben Luc – Long Thanh Expressway in Vietnam. The viaduct consists of 113 simply supported spans and one continuous bridge with a span arrangement of (86 + 140 + 86) m. The investigated pier caps were categorized into three categories: 92 piers supporting link slabs, 19 piers located at expansion joints, and two transition piers accommodating both Super-T girders and cast-in-place cantilever segments. During construction, visible cracking was identified in 87 of the 113 pier caps, which motivated the detailed field investigation reported in this paper.

An overview of the surveyed PPC pier caps is presented in Fig. 1. The layouts of the prestressing tendons and conventional reinforcement are illustrated in Figs. 2 and 3, respectively. The pier caps were designed using bonded post-tensioned tendons in combination with conventional reinforcement, with the amount and configuration of steel varying according to the structural function of each pier cap. In general, pier caps supporting link slabs were provided with twenty-three 32-mm-diameter reinforcing bars and four prestressing tendons, each consisting of twelve 7-wire strands with a nominal diameter of 15.2 mm. In contrast, pier caps at expansion joints or supporting girder segments were equipped with twenty-one 28-mm-diameter reinforcing bars and five identical prestressing tendons to accommodate higher force demands. The material properties of the concrete, reinforcing bars, and prestressing tendons used in the pier caps are summarized in Table 1. These properties were taken from the project specifications and were applied consistently in both the field interpretation and the numerical analyses.

(a) Overview of investigated pier

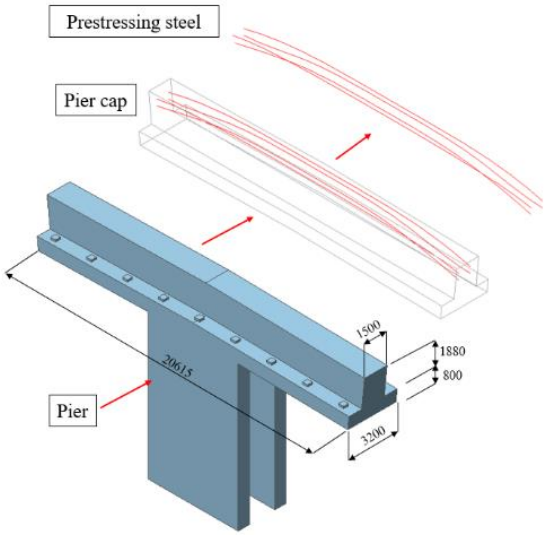

(b) 3D view of investigated pier and PPC pier cap

Fig. 1. Typical piers and PPC pier cap at expansion joints in Ben Luc – Long Thanh Expressway in Vietnam

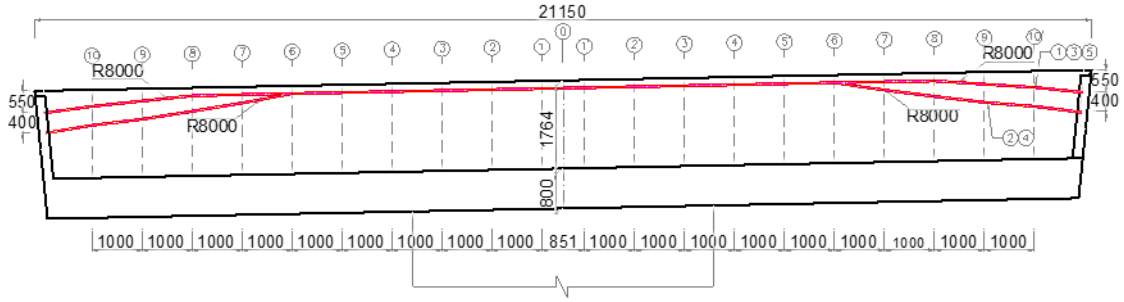

(a) Main view

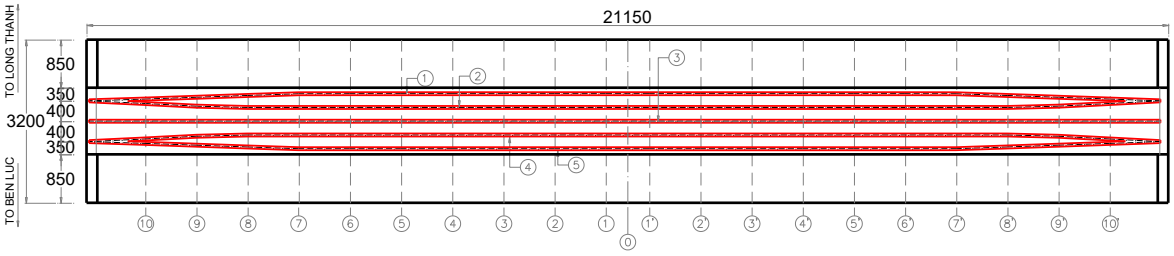

(b) Plan view

Fig. 2. Layout of prestressing tendons in a typical PPC pier cap

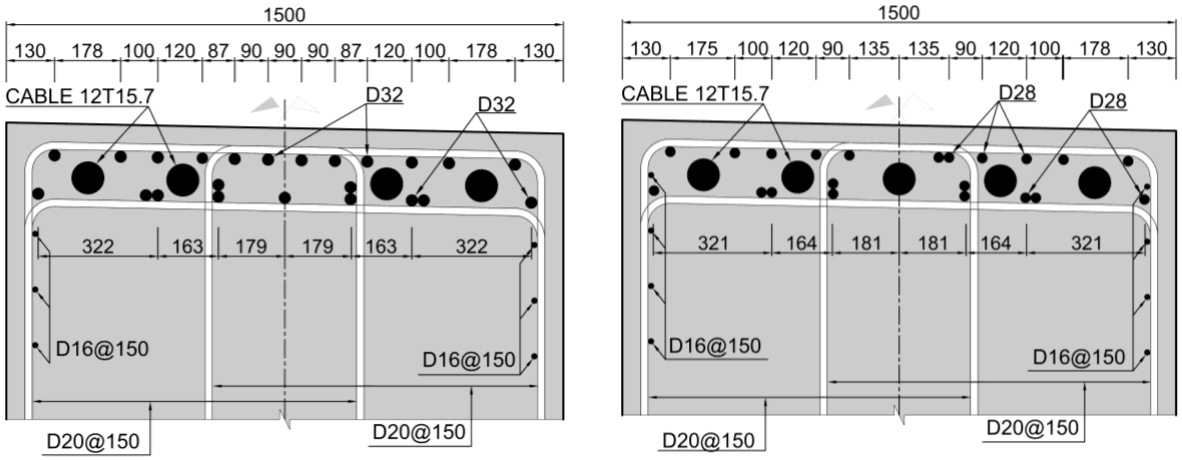

(a) Pier caps below link slab (b) Pier caps below expansion joint

Fig. 3. Layout of conventional reinforcement in a typical PPC pier cap

Table 1. Material properties of concrete, reinforcing bars, and prestressing tendons

Material	Type used	Density (kN/m^3)	Yield strength, f_y (MPa)	Ultimate strength, f_u (MPa)	Elastic Modulus, E (MPa)
Concrete	Compressive strength, $f'c$ = 30 MPa	24.5	-	-	29440
Reinforcing bars	CB400-V	78.5	400	570	200000
Prestressing tendons	Twelve 7-wire/low relaxation strands	77.1	1674	1860	197000

2.2. Field Inspection and Crack Measurement

Once the superstructure had been fully installed, visible cracks on the pier caps were systematically investigated to identify the characteristic cracking patterns of partially prestressed concrete

members. To provide a rigorous assessment of the cracking behavior of the partially prestressed pier caps, a detailed field survey was conducted on 24 piers selected randomly from the 87 pier caps in which visible cracking had been identified during the preliminary inspection stage. It should be noted that, due to limitations in site accessibility and inspection time, the selected sample represents approximately 25% of the cracked pier caps and was intended to reduce potential subjectivity and selection bias in the field investigation. Consequently, 24 out of the 87 cracked pier caps were examined in detail. Crack widths were measured using a specialized crack width gauge (ZBL-F130), as shown in Fig. 4(a), while crack depths were determined using an ultrasonic tester (C369N), as illustrated in Fig. 4(b).

(a) Measurement of surface crack width using ZBL-F130

(b) Measurement of crack depth using ultrasonic tester (C369N)

Fig. 4. Measurement of crack width and crack depth in the pier caps

2.3. Classification of Crack Patterns

Three representative crack types were identified, as illustrated in Fig. 5.

- Type 1 – Cracks at the cantilever–pier interface (ledge region):

Type 1 cracks develop along the vertical interface between the pier column and the overhanging cantilever part of the pier cap, where they are concentrated in the ledge region immediately above the pier shaft. These cracks propagate predominantly in a near-vertical direction and often extend upward into the body of the pier cap. Structurally, this region corresponds to the zone of maximum negative bending moment and high shear transfer between the pier and the cantilever arm. The combined effects of prestressing force, superstructure dead load, and column restraint generate high tensile stresses normal to the interface, making this region particularly susceptible to crack initiation and widening.

- Type 2 – Cracks in the stem of the pier cap above the pier:

Type 2 cracks occur in the stem (web) of the pier cap, which is located slightly above the cantilever–pier interface and extending upward into the main body of the pier cap. These cracks are generally inclined or vertical and are less frequent than Type 1 cracks. This region is governed by stress redistribution and local bending within the deep–beam zone of the pier cap. The presence of prestressing suppresses distributed cracking but promotes tensile strain localization in this transition zone, leading to the formation of discrete cracks in the stem, as confirmed by the nonlinear finite element results presented later.

- Type 3 – Cracks beneath bearing locations:

Type 3 cracks are vertical cracks directly beneath the bearing seats on the top surface of the pier cap. They initiate at the soffit of the bearing region and propagate downward into the pier cap. These cracks result from high local bearing pressures, transverse tensile splitting, and concentrated reactions transmitted from the superstructure. Under service loads, the combination of bearing pressure and restrained deformation generates tensile stresses perpendicular to the load path, producing vertical splitting cracks beneath the bearings.

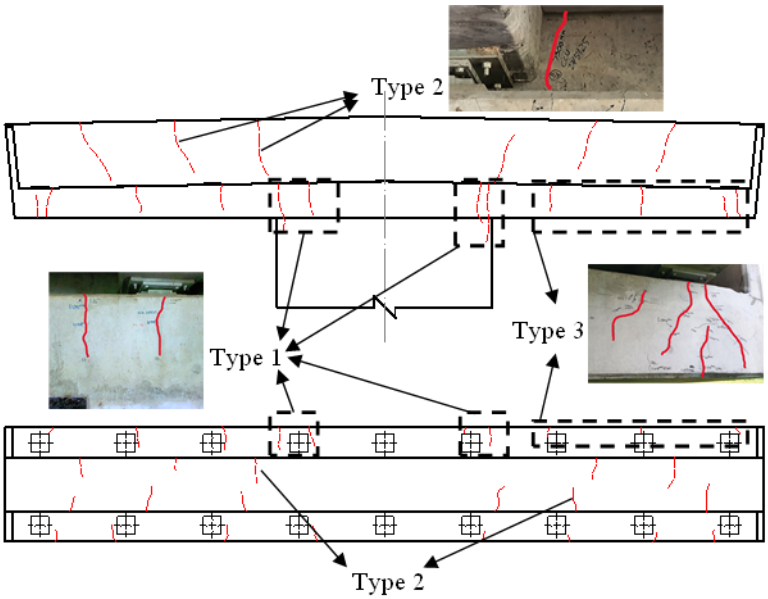

(a) Detailed crack patterns

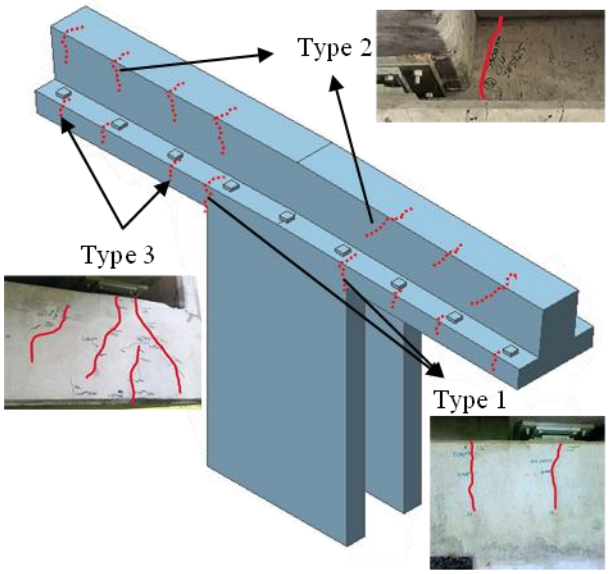

(b) Three-dimensional schematic view of crack patterns

Fig. 5. Observed crack patterns in PPC pier caps

Among the 24 surveyed cracked pier caps selected from the total population of 113 pier caps, a total of 426 cracks were recorded. Cracks occurring at the cantilever–pier interface (Type 1) and beneath the bearing zones (Type 3) were dominant, accounting for 74.9% and 20.7% of the total cracks, respectively, and were observed in nearly all of the pier caps. In contrast, Type 2 cracks represented only 4.5% of the total and were identified in just 5 of the 24 surveyed piers. Notably, these pier caps were all located at positions with link slabs, suggesting that restraint from the superstructure may play an important role in promoting crack development in this region.

2.4. Field Observations and Statistical Analysis of Cracking

2.4.1 Crack Patterns and Spatial Distribution

The overall distribution of measured crack widths is presented in Fig. 6. The results indicate that most cracks exhibited small crack openings, with 43.9% falling in the range of 0.1–0.2 mm and 29.6% being smaller than 0.1 mm. Cracks wider than 0.3 mm were relatively uncommon,

accounting for only 8.7% of all observations, while cracks exceeding 0.5 mm were negligible, representing just 0.2% of the total (a single crack).

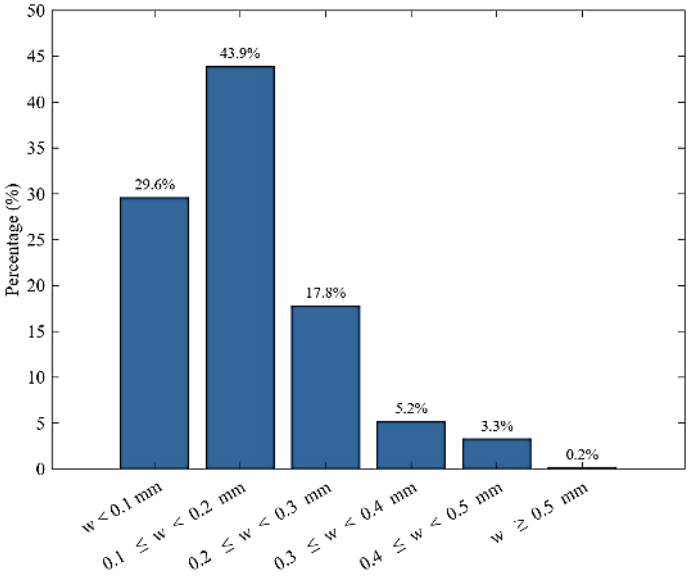

Fig. 6. Overall distribution of field-measured crack widths

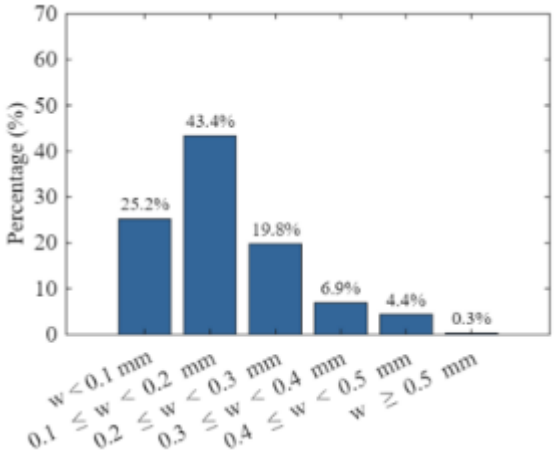

(a) Crack pattern 1

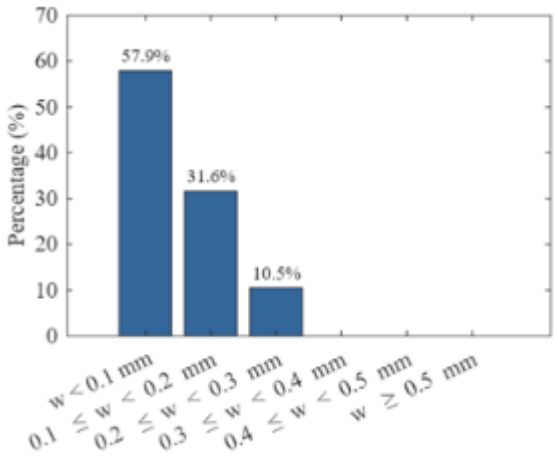

(b) Crack pattern 2

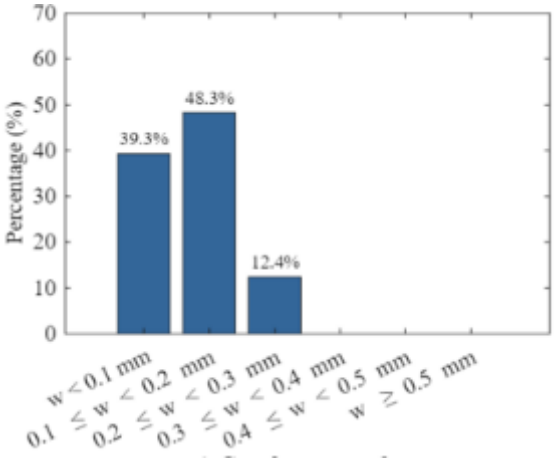

(c) Crack pattern 3

Fig. 7. Crack width distributions for the three crack patterns

The crack width distributions for the three crack types are shown in Fig. 7 and reveal clear differences in cracking behavior among the three regions of the pier caps. Cracks wider than 0.3 mm occurred exclusively in Type 1 cracks at the cantilever–pier interface; however, they accounted for less than 12% of this group, while the majority of Type 1 cracks (43.4%) remained in the 0.1–

0.2 mm range. This indicates that although wide cracks are more likely to develop in this highly restrained load-transfer zone, most cracks remain within moderate widths.

Type 2 cracks, located in the stem of the pier cap above the pier, were dominated by very small crack openings, with 57.9% of cracks smaller than 0.1 mm and 31.6% in the 0.1–0.2 mm range. Only 10.5% of Type 2 cracks exceeded 0.2 mm, reflecting the absence of strong strain localization in this region. A similar trend was observed for Type 3 cracks beneath the bearing zones, where 39.3% of cracks were smaller than 0.1 mm and 48.3% fell within the 0.1–0.2 mm range. Cracks wider than 0.2 mm accounted for only 12.4% of the population. This distribution suggests that although the bearing regions are subjected to high local stresses, the surrounding concrete provides sufficient confinement to limit crack opening.

Overall, the crack width distributions confirm that the cantilever–pier interface (Type 1) acts as the primary crack localization zone in PPC pier caps, whereas the stem and bearing regions tend to exhibit more distributed and finer cracking. The observed crack-width distribution exhibits a generally decreasing statistical trend, with the majority of cracks remaining below 0.2 mm and only a very limited number approaching or exceeding 0.5 mm. Although a single crack wider than 0.5 mm was identified, several additional cracks exhibited widths close to this threshold, indicating that the largest measured crack does not represent an isolated anomaly within the surveyed population.

2.4.2 Crack Depth Characteristics

Regarding crack propagation, the data summarized in Table 2 indicate that, for every surveyed pier, the maximum measured crack depth exceeded the nominal concrete cover thickness of 50 mm. In several pier caps, crack depths reached more than five times the cover thickness, with a maximum recorded value of 264.9 mm, indicating that cracks not only penetrated the cover layer but extended deep into the structural core of the pier caps.

Table 2. Maximum measured crack depths for the surveyed PPC pier caps

Pier Cap No.	Number of cracks measured	Number of vertical cracks	Number of inclined cracks	Maximum crack depth (mm)
P15	7	4	3	135.5
P16	6	6	0	155.9
P17	7	5	2	136.1
P19	5	5	0	172.3
P21	6	2	4	132.4
P22	5	2	3	187.5
P25	5	2	3	92.4
P26	5	2	3	69.2
P29	5	3	2	106.1
P30	5	3	2	125.7
P50	5	0	5	n.a
P51	7	6	1	129.9
P52	6	6	0	169.0
P55	5	4	1	122.6
P56	6	3	3	118.9
P59	8	2	6	168.9
P70	5	5	0	264.9
P71	7	7	0	207.0
P81	4	1	3	65.4
P82	5	3	2	114.3
P83	10	6	4	150.5
P85	7	6	1	173.9

This behavior is particularly critical for partially prestressed concrete members. Although prestressing reduces the number of surface cracks, it promotes crack localization, allowing individual cracks to propagate deeply once decompression is exceeded. Consequently, even cracks with relatively small surface widths can penetrate far beyond the cover depth, creating continuous

transport paths for moisture and chlorides toward the prestressing strands and conventional reinforcement. The field data therefore demonstrate that crack control based solely on surface crack width is insufficient to ensure durability in PPC pier caps. While a large proportion of the measured cracks had surface widths below 0.2 mm, their penetration depths frequently exceeded the protective cover by large margins, indicating a substantially higher corrosion risk than would be inferred from crack width alone.

The distinction between vertical and inclined cracks was introduced because depth measurements obtained from ultrasonic testing are considered more reliable for predominantly vertical cracks than for inclined cracks with irregular propagation paths. In addition, the reported crack depths are presented as absolute measured values and were primarily intended to assess whether the cracks had penetrated beyond the nominal concrete cover. A more detailed mechanics-based investigation relating crack propagation to member thickness and the effective tensile depth of the section is beyond the scope of the present study and is recommended for future research.

3. Numerical Study

To predict the structural response of the partially prestressed pier caps and to clarify the mechanisms governing crack development, a three-dimensional nonlinear finite element model was developed in this study. The model was used to simulate the effects of prestressing, dead load, and service load on crack initiation, propagation, and opening in the pier caps.

The analysis incorporates nonlinear material behaviour of concrete and steel and allows explicit simulation of cracking and tension stiffening degradation. This enables reproduction of the observed crack patterns and crack widths measured in the field, particularly in critical regions such as the cantilever–pier interface and beneath the bearing zones.

By comparing the numerical results with the field measurements, the finite element model provides both a predictive tool for evaluating crack development and a mechanistic framework for interpreting the cracking behaviour of PPC pier caps under service conditions.

3.1. Finite Element Model and Meshing

Fig. 8 shows the geometry and mesh of the finite element (FE) model. The concrete components were discretized using three-dimensional solid elements generated by extruding planar meshes along the longitudinal axis of the structure. Reinforcing bars and prestressing tendons were represented by one-dimensional embedded bar elements, whose material properties and cross-sectional areas were defined within the surrounding concrete elements to ensure strain compatibility and force transfer.

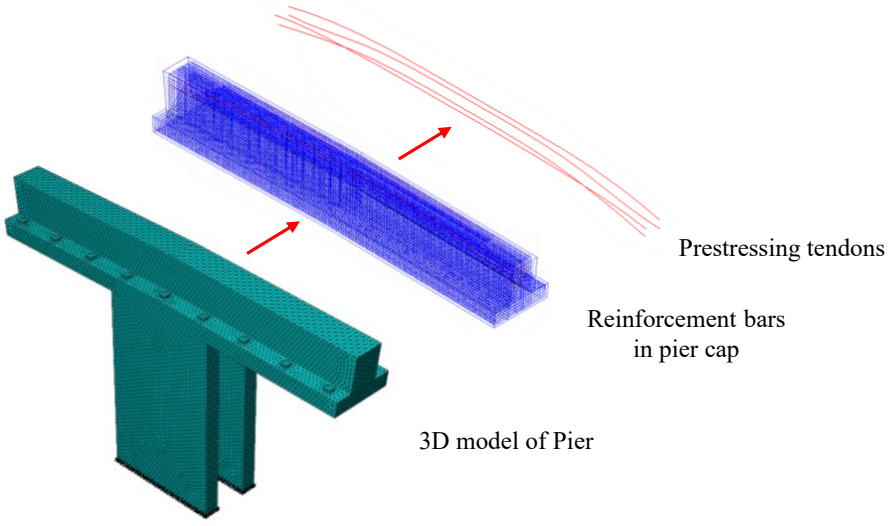

Fig. 8. Finite element model and mesh of the PPC pier cap

The computational domain was discretized using the automated Tetra Mesher in MIDAS FEA [20], which generates a variable-density tetrahedral mesh with smooth transitions between refined and coarse regions. To ensure adequate element quality, the meshing procedure employed an Optimization Level of 7, a Refinement Factor of 1.2, and a Shape Quality Weight of 7. The final FE model comprised 37,383 nodes and 177,871 elements. This mesh resolution was selected to be sufficiently fine in critical regions to accurately capture crack initiation, localization, and opening within the fracture-based concrete model.

3.2. Material Models

All structural components were modelled as isotropic in their initial (undamaged) state. The linear elastic properties of concrete and steel, including Young's modulus, Poisson's ratio, and mass density, were taken from the project design specifications as shown in Table 1.

To represent the nonlinear cracking and fracture behavior of concrete, the total strain crack model implemented in MIDAS FEA was adopted. Within this formulation, concrete is treated as initially isotropic, while anisotropy induced by cracking is captured through progressive stiffness degradation normal to crack planes. The compressive response of concrete was described using the Thorenfeldt stress–strain model [21], whereas the post-cracking tensile behavior was governed by the Hordijk softening law [22], which controls crack opening, tension stiffening, and energy dissipation (Fig. 9). The parameters defining these two constitutive relationships are provided in Table 3. It should be noted that in the Hordijk softening law, h denotes the crack band width, commonly taken as the representative element size in the fracture process zone. In this study, h is taken as 50 mm.

Reinforcing bars and prestressing tendons were modelled using a linear elastic constitutive relationship, which is appropriate for the serviceability limit state (SLS) considered in this study, where steel stresses remain well below yield and inelastic steel behavior is not expected to influence crack development. Under these conditions, crack initiation, propagation, and opening are governed primarily by the fracture behavior of concrete rather than by steel yielding.

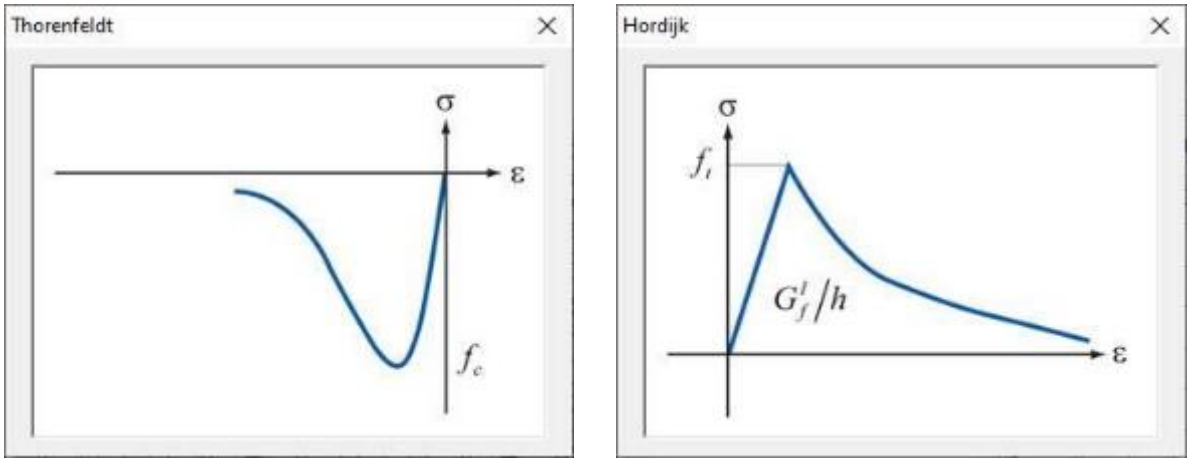

Fig. 9. Hordijk and Thorenfeldt models in Midas FEA

Table 3. Parameters for Thorenfeldt and Hordijk models

	Thorenfeldt's model	Hordijk's model		
Parameters	Compressive strength f'_c, N/mm2	Tensile strength f_t, N/mm2	Fracture energy G_f, N/mm	Crack band width h, mm
Value	35	3.2	0.084	50

3.3. Load and Boundary Conditions

Fig. 10 presents the boundary conditions, loading scheme, and interaction definitions adopted in the FE model. A perfect bond was assumed between concrete and both reinforcing bars and prestressing strands, enforcing full kinematic compatibility by tying the reinforcement nodes to the

surrounding concrete elements and preventing slip. This ensures that tensile forces are transferred to the steel as cracking develops in the concrete. The base of the pier was fixed to represent the foundation restraint. Self-weight was automatically applied based on the defined material densities. Superstructure loads, including dead and live loads, were obtained from an independent structural analysis and applied as pressure loads at the bearing areas. The prestressing action was introduced as an equivalent distributed pressure acting over the anchorage zones of the pier cap, representing the effective transfer of tendon forces into the concrete.

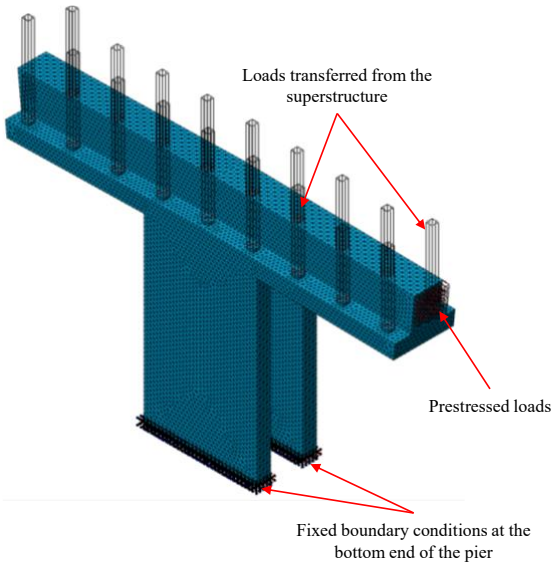

Fig. 10. Loads and boundary conditions

3.4. Numerical Validation and Analyses

Figs. 11 and 12 jointly illustrate the stress field and fracture response predicted by the fracture-based FE model. Fig. 11 shows the distribution of the first principal tensile stress in the concrete, revealing strong tensile stress concentrations at the cantilever–pier interface and beneath the bearing zones, which exhibit a strong spatial correlation with the cracking patterns observed in the field survey.

Fig. 12 presents the crack status predicted across the pier cap elements. In this representation, red regions denote fully open cracks, corresponding to zones undergoing tensile softening and progressive strength degradation. Blue regions indicate partially open cracks, where cracking has occurred but the material is in an unloading or reloading state, or within a transition regime of the fracture model. White regions represent uncracked elastic concrete, in which the tensile stress has not exceeded the cracking threshold. The presence of partially open cracks suggests that the prestressing force contributes to limiting crack opening by inducing localized unloading in the surrounding concrete, a behavior that is consistent with strain compatibility and tension-stiffening effects in prestressed members.

The FE analysis predicts two main regions of crack concentration: (i) the cantilever–pier interface and the bearing zones, where stress concentrations are expected to be high, and (ii) a more distributed cracking pattern along the pier cap stem. Field observations confirm the pronounced cracking at the pier cap ledge and bearing regions, whereas the stem cracking predicted by the model was observed less frequently, likely due to limited accessibility during on-site inspection.

Fig. 13 shows the predicted crack opening response under service loading, with a maximum crack width of 0.448 mm. This value is in good agreement with the field measurements, where most cracks were below 0.2 mm and only a single crack exceeded 0.5 mm, indicating that the fracture-based FE model captures the overall magnitude of crack opening reasonably well.

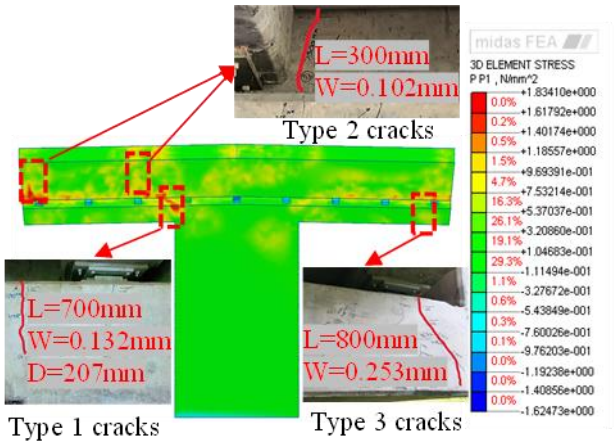

Fig. 11. First principal tensile stress distribution predicted by FE analysis

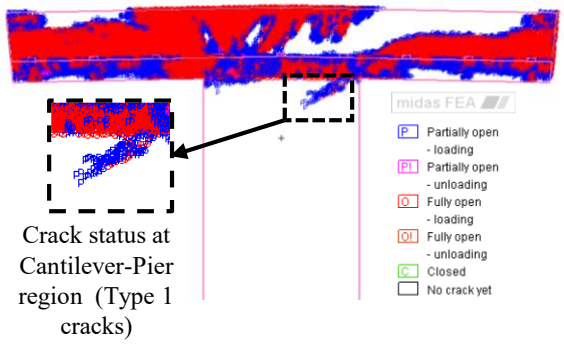

Fig. 12. Predicted crack status in the pier cap

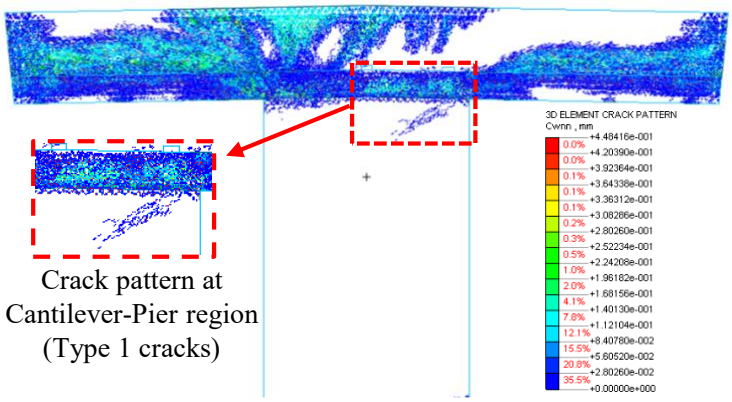

Fig. 13. Predicted crack opening width under service loading

Overall, the fracture-based FE analysis provides a physically consistent representation of crack initiation, localization, and opening in the PPC pier caps under service loading. While the model does not aim to reproduce every individual crack, it captures the dominant cracking zones and the upper bound of crack widths observed in the field, thereby offering a reliable framework for interpreting the measured crack patterns. This validated numerical representation forms a sound basis for assessing the adequacy of existing code-based crack control provisions, which is examined in the following section.

It should also be noted that the FE results represent a continuous crack-opening field throughout the concrete volume, including internal crack development, whereas the field survey is limited to discrete crack widths observable at the concrete surface. In addition, the field-measured cracks represent the accumulated structural response after construction and during service, including the effects of prestress transfer, self-weight, long-term restraint, creep, shrinkage, and traffic loading. Consequently, the FE model is not intended to reproduce the exact instantaneous in-situ crack state, but rather to capture the dominant crack localization mechanisms and upper-bound crack-opening behavior under service-level actions.

4. Crack Control According to Design Specification

The bridge investigated in this study was originally designed in accordance with TCN 272-05 [23], which is equivalent to the AASHTO LRFD bridge design specification [24]. In the present work, the code-based comparison is conducted using the ACI framework (ACI 318, ACI 224R, and ACI 350). This choice is motivated by the observation that the crack control provisions adopted in AASHTO LRFD are largely derived from, or calibrated against, ACI formulations. Accordingly, the ACI models provide a consistent and theoretically grounded basis for evaluating both the field measurements and the fracture-based FE predictions.

4.1. Background on Crack Control Provisions in the ACI Framework

Within the American design system, crack control in concrete structures is primarily governed by ACI 318 (Building Code Requirements for Structural Concrete). This standard is supported by a series of technical documents that provide the theoretical basis and interpretative guidance for cracking behavior, notably ACI 224R (Control of Cracking in Concrete Structures) and ACI 224.1R (Causes, Evaluation, and Repair of Cracks). For structures exposed to aggressive environments or requiring enhanced durability, more stringent crack control criteria are prescribed in ACI 350 (Code Requirements for Environmental Engineering Concrete Structures).

Together, these documents define the conceptual framework used in ACI-based design to limit cracking for durability and serviceability. However, the manner in which crack width is estimated and controlled within this framework has evolved significantly over time, particularly within ACI 318. This evolution is central to understanding the limitations of current crack control provisions when applied to partially prestressed concrete members.

4.1.1 Crack Control Philosophy in ACI 318

The crack control provisions in ACI 318 have undergone a fundamental conceptual shift over the past several decades. Prior to the 1999 edition, ACI 318-95 [25] adopted a direct crack width prediction approach based on the statistical model developed by Gergely and Lutz [26], in which the maximum surface crack width was expressed as a function of reinforcement stress and the geometry of the surrounding concrete. In this formulation, crack width was governed by the tensile strain in the reinforcement and the thickness and effective area of the concrete cover, reflecting a fracture-based view of cracking in reinforced and prestressed concrete:

$$w_{max} = 0.011 \times 10^{-3} \times \beta f_s \sqrt[3]{d_c A} \tag{1}$$

where f_s is the steel stress at service (MPa), d_c is the concrete cover to the nearest bar (mm), A is the effective tension area of concrete per bar (mm^2), and β accounts for the strain gradient. Under ACI 318-95, allowable crack widths were specified as 0.33 mm (0.013 in.) for exterior exposure and 0.41 mm (0.016 in.) for interior exposure, directly linking serviceability to crack opening.

However, subsequent research by Frosch [27] demonstrated that explicit crack width formulas exhibit large statistical scatter and limited predictive reliability. As a result, ACI 318-99 [28] abandoned the direct crack width calculation and replaced it with a spacing-based crack control model, in which crack width is no longer treated as an explicit response variable but is instead indirectly controlled through reinforcement spacing. In this physical interpretation, the average crack width is approximated as

$$w_{max} = 2 \frac{f_s}{E_s} \beta \sqrt{{d_c}^2 + \left(\frac{s}{2}\right)^2} \tag{2}$$

leading to reinforcement spacing limits of the form

$$s = \frac{95000}{f_s} - 2.5c_c \leq 300\left(\frac{252}{f_s}\right) \tag{3}$$

where s is the bar spacing and c_c is the concrete cover (mm). This approach implicitly assumes that limiting crack spacing is sufficient to control crack opening, without explicitly modeling fracture localization or tension softening.

This spacing-based philosophy remains the basis of crack control in ACI 318-19 [29], including for Class C partially prestressed members. For bonded prestressed reinforcement, the code limits the maximum spacing of steel closest to the tension face as

$$s = \frac{5}{6}\left[380\left(\frac{280}{\Delta f_{ps}}\right) - 2.5c_c\right] \tag{4}$$

or

$$s = \frac{5}{6}\left[300\left(\frac{280}{\Delta f_{ps}}\right)\right] \quad (5)$$

with the intent of maintaining crack widths below approximately 0.40 mm. Here, Δf_{ps} is the increase in prestressing steel stress beyond decompression (MPa).

4.1.2 Crack-Width Philosophy in ACI 224 and ACI 350

ACI 224R-01[30] provides a comprehensive framework for serviceability crack control by consolidating provisions from ACI 318, CEB-FIP, and Eurocode 2. In addition to code-based spacing rules, the document compiles several empirical and semi-mechanistic models for estimating maximum flexural crack widths in reinforced and prestressed concrete members. These include the formulations proposed by Meier and Gergely (1982) and by Nawy and Huang (1977) and Nawy (1989a), which are intended to relate crack width to steel stress, concrete cover, and effective tension area [31-33].

Meier and Gergely [31] proposed the following expressions for the maximum flexural crack width:

$$w_{max} = C_1 \frac{f_{ct}}{E_c} d_c \quad (6)$$

$$w_{max} = C_2 \frac{f_{ct}}{E_c} d_c \sqrt[3]{A} \quad (7)$$

where C_1 and C_2 are bond-related coefficients depending on the type of steel nearest the tension face; f_{ct} is the nominal tensile stress at the concrete tension (MPa); E_c is the concrete elastic modulus (MPa); d_c is the concrete cover to the centroid of the nearest reinforcement (mm); and A is the effective concrete tension area per bar (mm²) as defined in ACI 318 [28].

For prestressed members, ACI 224R-01 also includes simplified crack-width formulations derived by Nawy and Huang (1977) [32] and Nawy (1989a) [33], expressed in terms of the increase in steel stress beyond decompression:

Pretensioned members:

$$w_{max} = 5.85 \times 10^{-5} \frac{A_t}{\Sigma_0} \Delta f_s \quad (8)$$

Post-tensioned unbonded members:

$$w_{max} = 6.51 \times 10^{-5} \frac{A_t}{\Sigma_0} \Delta f_s \quad (9)$$

Where $\Delta f_s = f_{nt} - f_d$ is the increase in steel stress (ksi) relative to the decompression state, Σ_0 is the sum of reinforcement perimeters (in), and A_t is the effective concrete area in uniform tension (in²).

In the subsequent revision ACI 224.1R-07 [34], these empirical expressions were re-evaluated and largely superseded by the physically based crack model proposed by Frosch (1999), which relates crack width to reinforcement spacing and steel stress. ACI 350M-06 [35] adopts the same crack-width philosophy but introduces additional durability constraints by limiting the effective concrete cover used in crack-control calculations to a maximum of 50 mm.

4.1.3 Crack Control in AASHTO LRFD

The crack control provisions in the AASHTO LRFD Bridge Design Specifications closely follow the evolution of crack control philosophy in ACI 318. In the 2nd Edition (1998), AASHTO 1998 [24] adopted a stress-based crack width control approach derived from the Gergely–Lutz formulation [26], in which the allowable tensile stress in reinforcement was limited as a function of concrete cover and effective tension area in order to restrict surface crack widths to approximately 0.40 mm.

Beginning with the 3rd Edition, AASHTO 2004 [36] replaced this statistical crack-width formulation with the spacing-based physical model proposed by Frosch, consistent with the transition introduced in ACI 318. In the later version of AASHTO LRFD provisions [19, 37], crack control is governed primarily by the maximum spacing of reinforcement closest to the tension face, expressed as a function of steel stress, concrete cover, and an exposure factor. Crack width is no longer calculated explicitly but is assumed to be indirectly controlled through reinforcement spacing.

This evolution indicates that, as in ACI 318, AASHTO crack control for bridge structures has shifted from a fracture-based crack-width concept to a geometric spacing-based proxy, a simplification that may not fully capture the cracking behavior of partially prestressed bridge pier caps, where cracking, unloading, and re-opening are intrinsic to serviceability performance.

4.2. Comparison and Discussion

Table 4 summarizes the crack control verification of the investigated pier caps according to the maximum reinforcement spacing provisions in AASHTO LRFD and ACI 318. For all the investigated pier caps, the calculated bar spacing and steel stresses satisfy the code requirements. Under these provisions, compliance implies that surface crack widths should remain within approximately 0.40 mm at the serviceability limit state.

However, the direct crack-width evaluation presented in Table 5 for Pier P17 (the pier cap exhibiting the largest measured crack width) reveals a markedly different picture. Although this pier fully satisfies the spacing-based requirements of both AASHTO and ACI (Table 4), the fracture-based finite element model predicts a maximum crack width of 0.448 mm, while the field survey recorded a maximum surface crack width of 0.545 mm. Both values exceed the nominal serviceability limit of 0.40 mm, indicating that compliance with spacing-based crack control does not necessarily guarantee satisfactory crack performance for these partially prestressed pier caps. It is noted that the reported field maximum corresponds to the largest accessible crack, and additional cracking at the top surface of the pier cap may not have been fully captured.

Although cracks wider than 0.5 mm represent only a very small fraction of the total crack population (approximately 0.2% according to the distribution in Fig. 6), their occurrence is critical from a durability and serviceability standpoint. Crack control provisions in AASHTO and ACI are intended to limit the maximum crack width, rather than the average or most probable crack. The presence of even a single crack exceeding 0.5 mm in a pier cap that fully satisfies all code requirements indicates that the upper tail of the crack-width distribution is not adequately controlled by current spacing-based provisions. Nevertheless, several additional cracks exhibited widths close to the 0.5 mm threshold, and no abnormal cracking characteristics or visible construction deficiencies were identified in the corresponding pier caps during the field survey. This suggests that the occurrence of relatively large cracks is associated with localized structural response rather than with an isolated measurement anomaly.

In contrast, most of the traditional crack-width formulas summarized in Table 5, including those of Gergely–Lutz [26], Frosch [27], and Nawy & Huang [32], predict crack widths between 0.219 mm and 0.294 mm, well below the observed and numerically predicted values. This systematic underestimation is consistent with the empirical nature of these models, which were primarily calibrated using laboratory beams with relatively uniform stress fields and limited restraint, conditions that differ significantly from the deep, highly restrained, and prestressed pier caps examined in this study.

The only formulations that do not underestimate cracking are those proposed by Meier and Gergely [31], which predict crack widths of 1.097 mm and 2.270 mm, respectively. These values substantially exceed both the FEA and field measurements. This discrepancy is likely related to the fact that the Meier and Gergely equations were calibrated using laboratory beam tests characterized by moderate stress levels and distributed flexural cracking. In contrast, the investigated PPC pier caps exhibit highly restrained behavior and localized tensile stress concentrations near the crack localization zones. Based on elastic transformed-section analysis, the equivalent tensile stress associated with service-level cracking reaches approximately 32.3 MPa,

which lies well beyond the stress range represented in the original calibration database [31]. Consequently, direct application of these empirical equations to the investigated PPC pier caps may lead to unrealistic crack-width predictions.

More generally, the comparison between numerical predictions, code-based evaluations, and field observations should be interpreted within the limitations associated with in-service cracking measurements. Although the field-measured cracks represent accumulated in-service behavior rather than an instantaneous loading condition, the comparison remains valuable because both the FE analysis and the code-based crack-control checks were performed using consistent serviceability load combinations. The comparison therefore aims to assess whether current crack-control provisions can reasonably represent the magnitude and localization tendency of cracking observed in real PPC pier caps.

Taken together, the results in Tables 4 and 5 demonstrate a fundamental inconsistency between spacing-based crack control rules and the actual cracking behavior of partially prestressed pier caps. While current AASHTO and ACI provisions indicate full compliance, both field observations and fracture-based finite element simulations reveal crack widths that approach or exceed serviceability limits. This discrepancy highlights the limitations of indirect crack control based solely on reinforcement spacing when applied to large, deep, and highly restrained PPC members, and supports the need for fracture-informed or mechanics-based approaches to evaluate serviceability performance in such structures.

Table 4. Crack control verification according to ACI 318 and AASHTO LRFD

			Piers below Link Slab	Piers below Expansion Joint	P39
Reinforcement		Diameter (mm)	32	28	32
		Space (mm)	125	125	125
		Number	23	21	11
		d_c (mm)	84	84	84
		A (mm^2)	16663	18250	18273
		Z (N/mm)	23000	23000	23000
Service limit state		M (kN.m)	30695	30584	26406
		f_s (MPa)	209.1	217.6	185.5
	AASHTO 1998	f_{sa}	240	237	237
		Check	Compliant	Compliant	Compliant
	AASHTO 2007	β_s	1.046	1.048	1.028
		y_e	1	1	1
		smax (mm)	394	371	477
		Check	Compliant	Compliant	Compliant
	ACI 318-99	smax (mm)	244	227	302
		Check	Compliant	Compliant	Compliant
	ACI 318-19	smax (mm)	249	232	303
		Check	Compliant	Compliant	Compliant

Table 5. Comparison of crack width predictions and measured values for Pier P17

	Gergely and Lutz approach ACI 318-95	Frosch approach ACI 318-99	Meier and Gergely Equation (6)	Meier and Gergely Equation (7)	Nawy and Huang	Maximum crack width by FEM	Maximum crack width by on-site inspection
w (mm)	0.268	0.219	1.097	2.270	0.294	0.448	0.545

5. Conclusions

This study investigated the cracking behavior of partially prestressed concrete (PPC) pier caps based on an extensive field survey of 113 in-service bridge pier caps, complemented by nonlinear fracture-based finite element analysis and code-based crack control evaluation. The following conclusions can be drawn:

- Field inspections revealed that cracking is widespread in PPC pier caps designed in accordance with AASHTO LRFD and ACI provisions, with 87 out of 113 pier caps exhibiting visible cracks under service conditions. Although most cracks exhibited relatively small surface widths, the maximum measured crack width reached 0.545 mm, and crack depths consistently exceeded the nominal concrete cover thickness of 50 mm, indicating a potential durability concern.
- Three dominant crack patterns were identified: cracks at the cantilever–pier interface, cracks beneath bearing zones, and cracks in the pier cap stem. Among these, the cantilever–pier interface acts as the primary crack localization zone, accounting for the majority of observed cracks and the largest crack widths, highlighting the critical role of restraint and force transfer in PPC pier caps.
- The fracture-based finite element model successfully reproduced the dominant cracking zones observed in the field and predicted a maximum crack width of 0.448 mm under service loading. While the model does not aim to capture every individual crack, it provides a physically consistent representation of crack initiation, localization, and opening, and offers a reliable framework for interpreting field observations.
- Code-based crack control checks according to AASHTO LRFD and ACI 318 indicate full compliance for all investigated pier caps when assessed using reinforcement spacing limits. However, both field measurements and numerical simulations indicate that localized crack widths may approach or, in isolated cases, exceed the commonly adopted serviceability limit of 0.40 mm despite full code compliance. These findings suggest that spacing-based crack control may not always provide a reliable representation of crack localization behavior in PPC pier caps.
- Comparisons with empirical crack-width formulations compiled in ACI 224 show that most traditional models tend to underestimate crack widths for the investigated PPC pier caps, whereas some formulations calibrated outside the relevant stress range significantly overestimate cracking. These discrepancies reflect the limitations of empirical crack-width models when applied to large, deep, and highly restrained PPC members operating at high service-level stresses.

Overall, the results suggest that the cracking behavior of PPC pier caps may differ significantly from the assumptions embedded in current code-based crack control provisions. The combination of crack localization, deep crack penetration, and prestress-induced unloading cannot be fully captured by reinforcement spacing rules alone. These findings support the need for more mechanics-based approaches to assess serviceability and durability in partially prestressed bridge substructures.

Acknowledgement

This study was funded by Hanoi University of Civil Engineering, Vietnam, under project number 11-2026/KHXD-TĐ. The authors gratefully acknowledge the Vietnam Expressway Corporation (VEC) for providing access to the design documents and construction site, as well as for their valuable support throughout the research process.

References

[1] Bennett EW. Partial Prestressing-A Historical Overview. PCI J. 1984;29(5):104-117. https://doi.org/10.15554/pcij.09011984.104.117

[2] Chern JC, You CM, Bazant ZP. Deformation of progressively cracking partially prestressed concrete beams. PCI J. 1992;37(1):74-85. https://doi.org/10.15554/pcij.01011992.74.85

[3] Harajli MH, Naaman AE. Static and fatigue tests on partially prestressed beams. J Struct Eng. 1985;111(7):1602-1618. https://doi.org/10.1061/(ASCE)0733-9445(1985)111:7(1602)

[4] Au FTK, Du JS. Partially prestressed concrete. Prog Struct Eng Mater. 2004;6(2):127-135. https://doi.org/10.1002/pse.168
[5] Choudhary K, Akhtar S. Application of partial prestressing for crack control in reinforced concrete structures. In: AIP Conference Proceedings. Vol. 2158, No. 1. AIP Publishing LLC; 2019. https://doi.org/10.1063/1.5127151
[6] Huang Y, Wei J, Dong R. Stiffness of corroded partially prestressed concrete T-beams under fatigue loading. Mag Concr Res. 2020;72(7):325-338. https://doi.org/10.1680/jmacr.18.00187
[7] Guo W, et al. Experimental study on time-dependent behavior of partially prestressed concrete beams: Coupled effects of creep, cracking, and prestress loss. Eng Struct. 2026;351:122051. https://doi.org/10.1016/j.engstruct.2025.122051
[8] Witchukreangkrai E. Control of diagonal cracking in partially prestressed concrete beams. Proceedings of the Japan Concrete Institute. 2004;26(2):727-732.
[9] El Naas AA, El Hashimy HM, El Kashif KF. Comparative analytical study on crack width of reinforced concrete structures. Civil Eng J. 2021;7(07):1203-1221. https://doi.org/10.28991/cej-2021-03091720
[10] Terán-Torres BT, et al. Flexural stiffness and crack width of partially prestressed beams with unbonded tendons. Buildings. 2023;13(11):2717. https://doi.org/10.3390/buildings13112717
[11] Chowdhury S. Cracking and deflection behaviour of partially prestressed high strength concrete beams. In: Australasian Structural Engineering Conference (ASEC). The Meeting Planners; 2008.
[12] Khattab MM, Oukaili NK. Partially prestressed concrete beams under limited cycles of repeated loading. J Eng Sci Technol. 2019;14(2):966-983. https://doi.org/10.21660/2019.60.4514
[13] Kettelkamp J, Tuchscherer R. Estimating the Service-Level Cracking Behavior of Deep Beams. ACI Struct J. 2018;115(3):875-883. https://doi.org/10.14359/51702045
[14] Salem SH, et al. Experimental behavior of partially prestressed high strength concrete beams. Open J Civil Eng. 2013;3(3B):26-32. https://doi.org/10.4236/ojce.2013.33B005
[15] Dauji S, Bhargava K, Gupta D. Estimation of Flexural Crack Width in Reinforced Concrete Beams Using International Codes: A Parametric Analysis. Adv Civil Eng. 2025;2025(1):9961763. https://doi.org/10.1155/adce/9961763
[16] Cervenka V, et al. Simulation of the crack width in reinforced concrete beams based on concrete fracture. Theor Appl Fract Mech. 2022;121:103428. https://doi.org/10.1016/j.tafmec.2022.103428
[17] Accornero F, Cafarelli R, Carpinteri A. Cracking and crushing in prestressed concrete beams. ACI Struct J. 2021;118(2):101-109. https://doi.org/10.14359/51728184
[18] Liu D, et al. Crack-width prediction model and rapid design method for partially prestressed concrete beams using boosting framework. Eng Struct. 2025;329:119854. https://doi.org/10.1016/j.engstruct.2025.119854
[19] American Association of State Highway and Transportation Officials (AASHTO). AASHTO LRFD Bridge Design Specifications. Washington, DC: AASHTO; 2017.
[20] MIDAS Information Technology Co., Ltd. MIDAS FEA NX: Advanced Nonlinear and Detailed Analysis Software. Seongnam, South Korea; 2016.
[21] Thorenfeldt E. Mechanical properties of high-strength concrete and applications in design. In: Symposium Proceedings, Utilization of High-Strength Concrete. Norway; 1987.
[22] Hordijk DA. Local approach to fatigue of concrete [Dissertation]. Delft: TU Delft, Delft University of Technology; 1991.
[23] Ministry of Transport (MoT). 22TCN 272-05: Regulations on Design of Concrete & Composite Bridges (in Vietnamese). Hanoi, Vietnam: MoT; 2005.
[24] American Association of State Highway and Transportation Officials (AASHTO). AASHTO LRFD Bridge Design Specifications. Washington, DC: AASHTO; 1998.
[25] American Concrete Institute (ACI). Building code requirements for structural concrete (ACI 318-95). Farmington Hills, MI: ACI; 1995.
[26] Gergely P, Lutz LA. Maximum crack width in reinforced concrete flexural members. Special Publication. 1968;20:87-117.
[27] Frosch RJ. Another look at cracking and crack control in reinforced concrete. ACI Struct J. 1999;96(3):437-442. https://doi.org/10.14359/679
[28] American Concrete Institute (ACI). Building code requirements for structural concrete (ACI 318-99). Farmington Hills, MI: ACI; 1999.
[29] American Concrete Institute (ACI). Building code requirements for structural concrete (ACI 318-19). Farmington Hills, MI: ACI; 2019.
[30] American Concrete Institute (ACI). Control of cracking in concrete structures (ACI 224R-01). Farmington Hills, MI: ACI; 2001.
[31] Meier SW, Gergely P. Flexural Crack Width in Partially Prestressed Concrete Beams. J Struct Div. 1981;107(2):429-433. https://doi.org/10.1061/JSDEAG.0005651

[32] Nawy EG, Huang PT. Crack and deflection control of pretensioned prestressed beams. PCI J. 1977;22(3):30-47. https://doi.org/10.15554/pcij.05011977.30.47
[33] Nawy EG. Flexural cracking behavior of partially prestressed pretensioned and post-tensioned beams-State of the art. Cracking in prestressed concrete structures, SP 113. 1989;1-28.
[34] American Concrete Institute (ACI). Control of cracking in concrete structures (ACI 224R-07). Farmington Hills, MI: ACI; 2007.
[35] American Concrete Institute (ACI). Code Requirements for Environmental Engineering Concrete Structures and Commentary (ACI 350M-06). Farmington Hills, MI: ACI; 2006.
[36] American Association of State Highway and Transportation Officials (AASHTO). AASHTO LRFD Bridge Design Specifications. Washington, DC: AASHTO; 2004.
[37] American Association of State Highway and Transportation Officials (AASHTO). AASHTO LRFD Bridge Design Specifications. Washington, DC: AASHTO; 2024.